Materials Research Express

PAPER

Effect of different hardness and melting point of the metallic surfaces on structural and optical properties of synthesized nanoparticles

To cite this article: Ke Zhang *et al* 2019 *Mater. Res. Express* **6** 045027

Materials Research Express

PAPER

Effect of different hardness and melting point of the metallic surfaces on structural and optical properties of synthesized nanoparticles

Ke Zhang[1,2], **Rashid A Ganeev**[1], **Ganjaboy S Boltaev**[1], **Pavel V Redkin**[1] and **Chunlei Guo**[1,3]

[1] The Guo China-US Photonics Laboratory, State Key Laboratory of Applied Optics, Changchun Institute of Optics, Fine Mechanics, and Physics, Chinese Academy of Sciences, Changchun 130033, People's Republic of China
[2] University of Chinese Academy of Sciences, Beijing 100049, People's Republic of China
[3] The Institute of Optics, University of Rochester, Rochester, NY 14627, United States of America

E-mail: rashid_ganeev@mail.ru **and** guo@optics.rochester.edu

RECEIVED
28 November 2018

REVISED
21 December 2018

ACCEPTED FOR PUBLICATION
4 January 2019

PUBLISHED
16 January 2019

Keywords: laser ablation in liquids, metal nanoparticles, nonlinear optical properties

Abstract

The relations between macroscopic and microscopic characteristics of materials are of utmost importance for synthesis of multi-atomic structures with advanced properties. We analyze the influence of pulse duration, pulse energy and temperature of liquid on the process of formation of nanoparticles (NPs) of the metals (In, Sn, Zn and W) with different hardness and melting temperature by laser ablation in liquid environment. Composition, morphology dynamics and properties of nanoparticle suspensions are studied using TEM analysis and Z-scan technique. The nonlinear optical properties of NPs are analyzed at 800 and 400 nm using 60 fs and 200 ps pulses. We show that pulse energy have little influence on the formation, morphology and size of NPs during ablation of low hardness and melting point metal (In). However, pulse duration plays a very important role during the formation of NPs, especially the ultra-short pulse has a positive effect on the preparation of NPs with smaller particle size. In addition, the temperature of liquid environment influences the formation of NPs and their nonlinear optical properties.

1. Introduction

Nanoparticles (NPs) are extensively researched because of their promising applications in sensors, nanophotonics and materials with new properties [1–8]. Metal NPs of In, Sn, Zn and W with different hardness, melting and boiling points, represented by, have been widely used in photoelectron and chemical industries [9, 10], ultraviolet photo detectors [11, 12], sensing devices [13–17], super capacitors [18], new materials [19–21], photonics [22], biomedical applications [23, 24], etc.

Currently, the synthesis of NPs mainly includes sol-gel technology [25], thermal decomposition [26], microwave - assisted production [27], reactive magnetron sputtering [28], pulsed laser deposition [29, 30], and pulsed laser ablation [31–34]. The synthesis of metal and metal oxide NPs by laser ablation in liquid environment is also an example of 'green' nanotechnology. Many factors, such as the temperature of liquid, the duration, intensity, wavelength, polarization, and repetition rate of the laser pulse, make it possible to control the morphology and size of the NPs. In-depth research and analysis of characteristics of NPs greatly increases their application area. In, Sn, Zn and W are chemically active, and can be easily oxidized in water, especially due to laser ablation. So, it is doubtable if the ablated NPs are still metal-only. Laser ablation-induced oxidation of metal NPs in water was reported in [10, 22, 33].

We studied the formation of NPs of metals with low and high melting point, boiling point and hardness (In and W, correspondingly). We also analyzed ablation of Sn and Zn, which possess intermediate characteristics. We study the dependence of nonlinear optical characteristics of synthesized NPs on these macroscopic properties of bulk materials.

Table 1. Parameters of pulses used for laser ablation.

Laser	Pulse duration	Wavelength (nm)	Repetition rate (Hz)
Nd:YAG	5 ns	1064	10
Ti:sapphire	200 ps	800	1000
	60 fs	800	1000

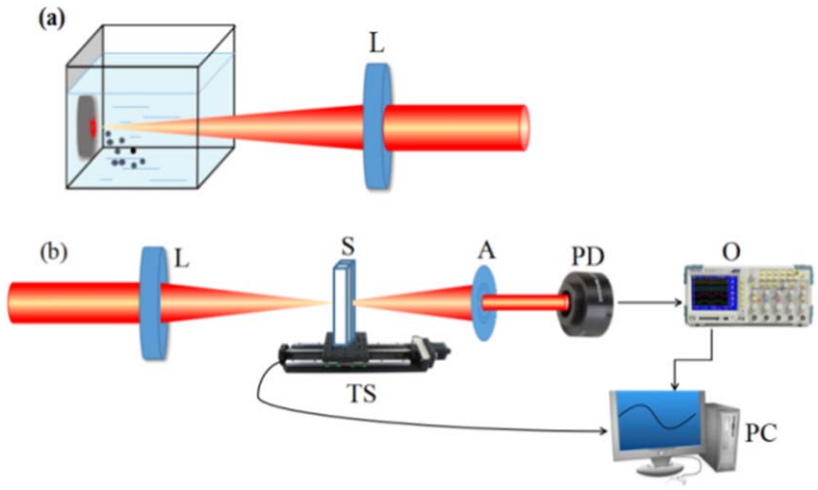

Figure 1. Experimental layouts for (a) laser ablation of metals in liquid environment and (b) Z-scan studies. (a) L: lens, f = 150 mm. (b) L: lens, f = 400 mm, S: sample, A: aperture, PD: photodiode, O: oscilloscope, PC: computer, TS: translation stage.

Table 2. Parameters of laser ablation of In target.

Used pulses	Sample	Pulse energy (mJ)	Fluence (J cm^{-2})	Intensity ($\times 10^{11}$ W cm^{-2})	Duration of ablation (min)	Temperature of liquid (°C)
5 ns	In-ns	30	667	1.3	10	20
200 ps	In-ps	0.54	12	0.6		
60 fs	In-fs	0.54	12	2000		
200 ps	In-ps01	0.53	12	0.6	15	
	In-ps02	0.45	10	0.5		
	In-ps03	0.29	6.4	0.32		
	In-ps04	0.25	5.6	0.28		
	In-ps05	0.15	3.3	0.17		
	In-ps06	0.04	0.9	0.05		
200 ps	In-low	0.54	12	0.6	15	4
	In-high		12	0.6		80

2. Experimental arrangements

A 150 mm focal length lens was used to focus laser pulses on the surface of the metal targets, which were placed in a 30 mm long quartz cell containing 10 ml of distilled water. Quartz cell was moved along the X-Y directions during ablation, and the target was placed 25 mm away from the input window. The diameter of the focusing spot after focusing was 76 μm. The parameters of the used pulses are shown in table 1. The experimental setup is shown in figure 1(a).

We studied the influence of pulse duration, pulse energy and temperature of the liquid on the formation of NPs of In as a metal with low hardness, melting and boiling points. The relevant parameters are shown in table 2. In addition, several other metals (Sn, Zn and W) with higher hardness, melting and boiling points were also used in these studies. The parameters of laser ablation of Sn, Zn and W are shown in table 3. The fluence of laser radiation on the target surface was determined by measuring the laser energy of each pulse and the spot area of the beam. It is noteworthy that the pulse energy mentioned in the table is the total energy of each single pulse. In

Table 3. Parameters of ablation of Sn, Zn and W targets.

Target	Used pulses	Sample	Pulse energy (mJ)	Fluence (J cm^{-2})	Intensity ($\times 10^{11}$ W cm^{-2})	Duration of ablation (min)
Sn	5 ns	Sn-ns	52	1160	2.32	40
	200 ps	Sn-ps	0.54	12	0.6	
	60 fs	Sn-fs	0.87	19	3170	
Zn	5 ns	Zn-ns	102	2267	4.53	20
	200 ps	Zn-ps	0.54	12	0.6	
	60 fs	Zn-fs	0.87	19	3170	
W	5 ns	W-ns	52	1160	2.32	80
	200 ps	W-ps	0.54	12	0.6	40
	60 fs	W-fs	0.87	19	3170	40

addition, in order to facilitate comparison, the corresponding fluence and intensity of focused beam are presented.

Nonlinear optical properties of ablated samples were studied using the standard Z-scan technique [35]. Before the Z-scan measurements we analyzed the spatial characteristics of probe beams using a CCD camera (Thorlabs) and confirmed that the beam profiles in the focal area were close to Gaussian, which is a prerequisite for the analysis of Z-scan traces using the relations developed for this technique. The laser pulse was focused by a lens with a focal length of 400 mm, and then the radiation was transmitted through the sample (2-mm-thick cell filled with NPs suspension) and measured by a broad-area photodiode (figure 1(b)). The description of our scheme is reported in [36].

The nonlinear absorption coefficients (β) of these samples were calculated from the open-aperture (OA) Z-scan curves. To obtain closed-aperture (CA) Z-scans, the aperture in front of photodiode was partially closed to allow 10% of incident energy pass towards the photodiode. The CA Z-scan curve allowed determination of both β and nonlinear refractive index (γ) of the analyzed samples. The 400 nm radiation (second harmonic of 800 nm pulses) was used to study the effect of wavelength on the nonlinear optical properties of metal NPs suspensions.

3. Morphology and optical characterization of NPs

These colloidal suspensions obtained at different heating pulse duration, pulse energy and liquid temperature were analyzed by ultraviolet-visible (UV–vis) absorption spectrometry (Cary Series, Agilent Technologies), scanning electron microscopy (SEM, S-4800, Hitachi) and transmission electron microscopy (TEM, JEM 2100F, Jeol) to determine the surface plasmon resonances (SPR), morphology, size of particles and distribution of NPs correspondingly. In order to analyze the chemical composition and microcosmic structure of NPs, x-ray Diffraction (XRD, D8 Discover, Bruker AXS) was carried out in the case of In NPs. Indium, as a very soft metal (Mon's hardness: 1.2), has a very small melting point (156.76 °C). Its heat of melting and heat of evaporation are 3.263 kJ mol^{-1} and 231.5 kJ mol^{-1} respectively. Obviously, indium is a very easily ablated metal. The SEM studies of NPs suspensions showed that the morphology of these samples was changed during a few days after ablation. The initial NPs showed regular spherical shape with broad size distribution for different pulse duration (5 ns, 200 ps and 60 fs), ablation energy and different temperatures (high and low) of distilled water (figure 2(a)). Surprisingly, after a few days their morphology changed towards the cubic and rectangular structures with narrower size distribution, while the suspensions still contained a small amount of spheroid and rod-like particles (figure 2(b)).

The initial morphologies of NPs prepared by ns and ps pulses, including ps ablation with different energies and different water temperatures are similar. They all show regular spherical structure at first, and the cube-like shape structure appear after several days of aging. In the following months the morphology and size of particles remained stable. The nonlinear optical properties of NPs suspensions were carried out at this stage of cubic morphology.

In the case of different pulse durations, the morphology and size of NPs obtained by ns and ps pulses (both at the beginning of ablation and after aging) were not significantly different, that is, the single pulse of 200 ps and 5 ns have basically the same influence on the ablation and further morphology modification in the case of In. This is mainly due to the low hardness, melting and boiling point of In target, the low sensitivity to external ablation environment, and similar ablation effect can be achieved at different ablation conditions.

In addition, it is worth noting that in the case of ps pulses with different energies. SEM images show that the change of ablation energy did not make a significant difference in morphology and size of NPs. There are two main reasons for this result. On the one hand, it is easy to find although all of them, a single pulse energy, fluence

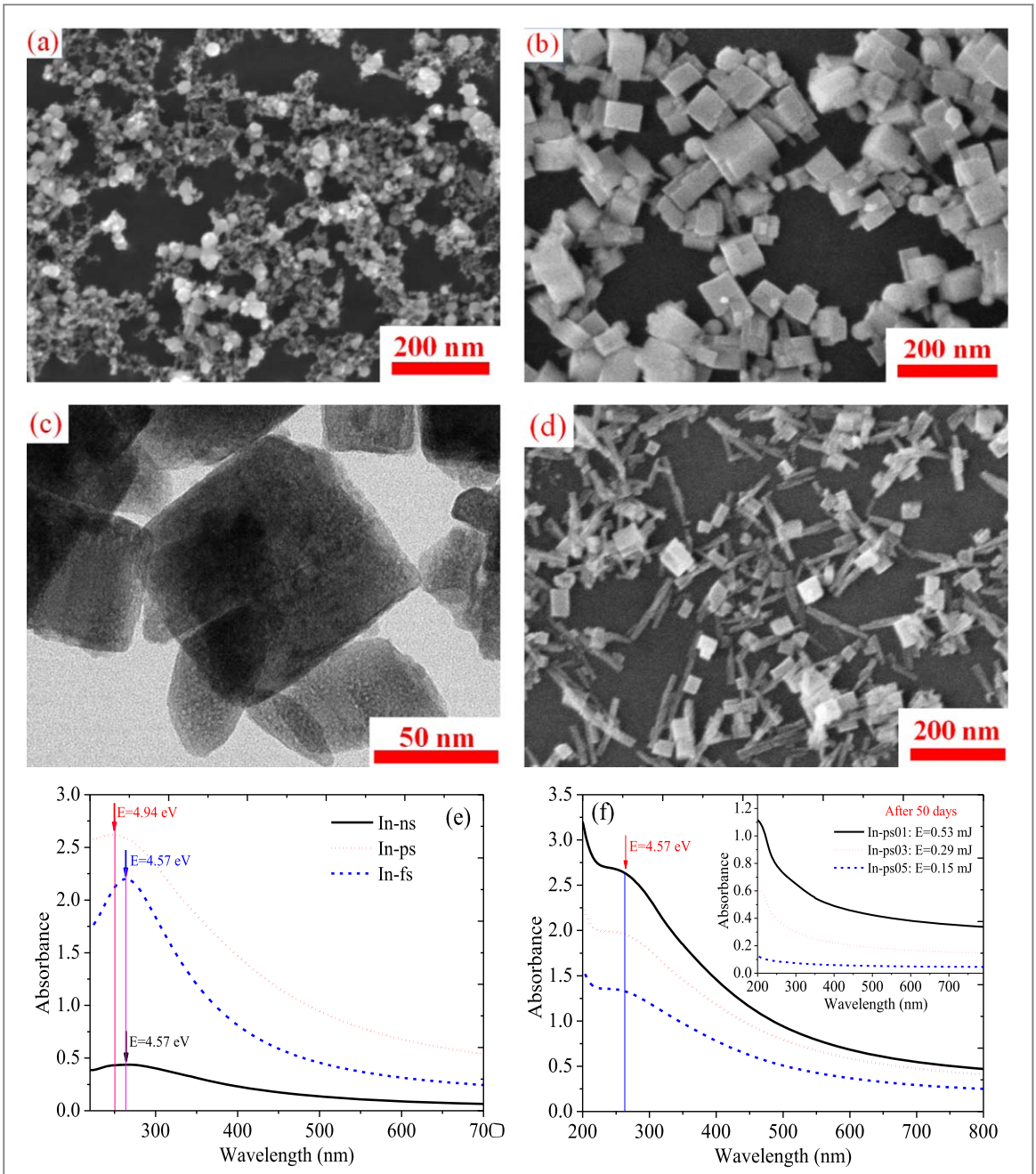

Figure 2. (a) SEM image of initial In NPs obtained by ps (pulse duration: 200 ps, wavelength: 800 nm, pulse energy: 0.54 mJ, duration of ablation: 10 min) and ns (pulse duration: 5 ns, wavelength: 1064 nm, pulse energy: 30 mJ, duration of ablation: 10 min) pulses. (b) SEM image of the same suspension after two days. (c) TEM image of cuboid In NPs obtained using ablation by ps pulses (pulse duration: 200 ps, wavelength: 800 nm, pulse energy: 0.54 mJ, duration of ablation: 10 min). (d) SEM image in the case of ablation by fs pulses (pulse duration: 60 fs, wavelength: 800 nm, pulse energy: 0.54 mJ, duration of ablation: 10 min). (e) Absorption spectra of the aqueous solutions of In NPs obtained by different pulse duration (5 ns, 200 ps and 60 fs). (f) Absorption spectra of the aqueous solutions of In NPs synthesized by ps pulses with different energies. Inset: absorption spectra of the same suspensions after 50 days.

or intensity have difference, showing a decrease trend, there are no significant differences in magnitude of those parameters (see table 2). That is to say, for the ablation of In target, the change of pulse energy in a small range cannot bring observable effect on ablation. On the other hand, In is a very soft material, with low melting and boiling points and, hence, low ablation threshold. Thus the lower ablation energy can lead to the same effect as the high energy of heating pulses.

More importantly, while comparing the ablation by ns and ps pulses, one can find that the ablation intensity of ns pulses is not significantly different from that of ps pulses, but the fluence of ns pulses is notably larger than that of ps pulses. In spite of a large difference between the fluences of ns and ps pulses, the consistency of morphology and particle sizes seem to imply that the fluence does not has a decisive effect on the ablation of the studied metal targets.

TEM studies of particles obtained by ps pulse are shown in figure 2(c). There were no obvious lattice structures and the corresponding interference patterns. However, the results of ablation in the case of short pulse duration (60 fs) were significantly different. In the case of fs pulses just after ablation its morphology was not significantly different from that of the former two cases, but after several days of aging most of its particles had rod-shaped structures and some of the smaller sized cubic and rod-like structures(figure 2(d)). Compared with the former cases (i.e. ns and ps pulses), the particle size was significantly reduced. Obviously, this effect is mainly caused by the pulse duration, thus pointing out that the use of ultra-short pulses plays an important role in synthesizing smaller-sized NPs.

The initial absorption spectra of aqueous suspensions of In NPs produced by ablation of In bulk using laser pulses of different duration are shown in figure 2(e). The SPR peak was located at $\lambda \approx 260$ nm (E = 4.57 eV). The result is consistent with the SPR peak of In NPs obtained by chemical methods [37]. The plasma resonance peak of In NPs with chloroform as dispersant has been reported at 240 nm in [38]. This difference is mainly due to the effect of the solvent. It has been reported that the position of the SPR peak is strongly dependent on the solvents [39], morphologies [40] and size [41] of the NPs. However, compared to chemical synthesis, pulsed laser ablation in liquid environment provides a green, safe and efficient synthesis. The shapes of absorption curves and peak positions of SPR were similar to each other. However, the absorption of the In suspensions obtained by ps and fs pulses was significantly stronger than in the case of ns pulses, mainly because the repetition rate of the former pulses (1 kHz) was significantly higher than that of the latter pulses (10 Hz). Therefore, the number of ablation ns pulses was significantly smaller during the same ablation time.

In the case of ablation of In by ps pulses the absorption spectra of In NPs were analyzed using different energies of laser pulses (figure 2(f)). Their absorption spectra after 50 days from ablation are shown in the inset of figure 2(f). In the latter case, one can see the disappearance of the peak related with the SPR of In. The possible factors leading to the disappearance of peak were mainly caused by the change of the morphology and chemical composition during aging. Obviously, these two factors coexist during the aging process.

The height of SPR peak depended on the pulse energy during ablation (figure 2(f)). The larger pulse energy led to larger concentration of small-sized particles at the same ablation time that led to higher absorption along the whole spectral range. The SEM images showed that the initial morphology and sizes of spherical particles obtained using different pulse energies were approximately the same. This similarity led to insignificant difference in the position of SPR.

Note the dramatic change of NPs morphology over time. A few days after the end of ablation the samples showed significant aggregation in square-like, cubic and rectangular forms, thus erasing the difference in ablation conditions. Particularly, they did not show a dependence on the energy used in preparation. The continuous SEM tests showed that no significant difference in morphology and size of particles in the three following months after the formation of the cubic particles had occurred. At that time the SPR entirely disappeared from the absorption spectra (see inset in figure 2(f)).

Sn is also a soft metal, while it has slightly larger hardness compared with In (Mon's hardness: 1.5). Melting and boiling points of Sn are 232 °C and 2260 °C respectively. Compared with the former, Zn is relatively hard (Mon's hardness: 2.5), and the melting point of Zn is 419.53 °C, that is higher than those of the first two metals. The results of SEM (figure 3(a)) and TEM (inset of figure 3(a)) studies showed that the size of Sn NPs varied from 4 to 8 nm, and there were obvious lattice related interference patterns. Note that the results of ablation using ns and ps pulses showed no significant difference in size and morphology of NPs, but the NPs obtained at fs conditions were relatively smaller. This conclusion is completely consistent with what we seen in the former case, which is an additional confirmation of the conclusion that the ultra-short pulses allow obtaining smallest NPs. Compared with In, Sn NPs were not changed significantly during a few days after ablation, and their spherical shape and size of particles remained stable in the next few months. Their nonlinear optical characterization was carried out at the condition of completely stabilized morphology. Later, significant aggregation appeared, being more prominent with the passage of time.

As a relatively hard metal, Zn ablated by pulses of different duration demonstrated a difference from the previous two metals. The most obvious feature is that the pulse duration has a significant effect on the synthesized particles' sizes. The particles, which were prepared using different duration of pulse, showed irregular fracturing morphology. This is what they have in common in terms of morphology. The effect of pulse duration is mainly influences the particles' sizes. In the case of ns pulse, the size distribution of particles was extremely broad, ranging from several nanometers to nearly 100 nm. The size distribution of particles was relatively narrower during ablation using ps pulses (10–40 nm). This trend was more significant when fs pulses were used. Interestingly, after nearly two months of aging the Zn NPs showed significant changes in morphology, presenting a cubic structure and a significant increase in size of particles (inset of figure 3(b)).

The absorption spectra of initial Sn and Zn NPs suspensions were carried out immediately after the ablation using the pulses with different durations. Additionally, their absorption spectra after 50 days are shown in figures 3(c) and (d) respectively. The hardness, melting point and boiling point of these metals is average among

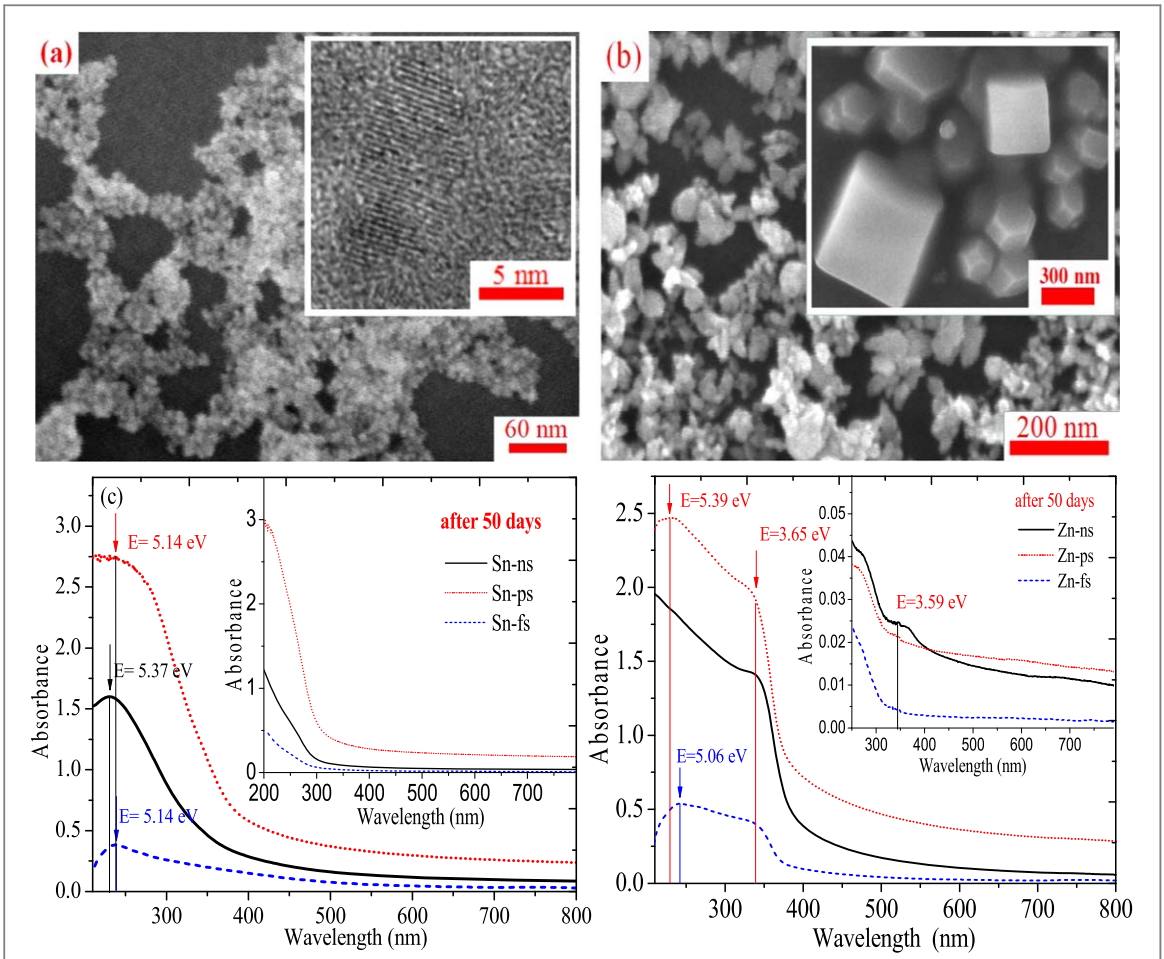

Figure 3. (a) SEM image of Sn NPs obtained using ps pulses (pulse duration: 200 ps, wavelength: 800 nm, pulse energy: 0.54 mJ, duration of ablation: 40 min). Inset: TEM image of the same species. (b) SEM image of Zn NPs obtained using ps pulses (pulse duration: 200 ps, wavelength: 800 nm, pulse energy: 0.54 mJ, duration of ablation: 20 min). The morphology and size of particles remained stable for two months. Inset: SEM results after two months. (c) Absorption spectra of aqueous solutions of Sn NPs obtained at different pulse durations (5 ns, 200 ps and 60 fs). Their SPR peak position was at $\lambda = 240$ nm (E = 5.14 eV). Inset: absorption spectra after 50 days. (d) Absorption spectra of the aqueous solutions of Zn NPs obtained at different pulse durations (5 ns, 200 ps and 60 fs). Their SPR peak positions were at $\lambda = 230$ nm (E = 5.39 eV) and $\lambda = 340$ nm (E = 3.65 eV). Inset: absorption spectra after 50 days.

the four chosen species. In the case of Sn NPs suspension their SPR was at about $\lambda = 240$ nm (E = 5.1 eV). Compared with the former two metals, Zn is a special case, and there are two resonance peaks. The first is at $\lambda \approx 235$ nm (E $\approx$ 5.2 eV), and the second is at $\lambda = 340$ nm (E = 3.7 eV). The second one (E = 3.7 eV) is well consistent with the absorption of ZnO [42–45]. The mixture of Zn and ZnO was be obtained by ablation Zn target in liquid environment. The results are in good agreement with [46] .

W is a metal with very high Mon's hardness (7.5). Compared to the preceding metals, W has very high melting (3410 °C) and boiling (5927 °C) points. Because of this, ablation of W is very difficult. At present, W NPs are mainly produced by chemical synthesis methods, such as magnetron sputtering, gas aggregation [47, 48], selective precipitation [49], reverse micelle method [50], solvothermal decomposition [51], plasma expansion [52]. SEM image of W suspension showed the presence of 10 to 30 nm sized NPs, which were not changed with the time (figure 4(a)). This is mainly due to the fact that W is difficult to hydrolyze or oxidize with water and oxygen at this experimental condition, so the morphology of particles formed by plume cooling has better stability. The initial absorption spectra of W NPs were studied in the case of different pulse durations, and their absorption spectra after 50 days of aging shown in figure 4(b). The absorption spectra of the solution of NPs obtained using ps pulses had SPR peak at $\lambda \approx 320$ nm (E = 3.86 eV). After 50 days the SPR peak had a strong blue shift ($\lambda \approx 260$ nm, E = 4.75 eV).

In order to analyze the chemical composition of the NPs, XRD was carried out for the In NPs, which were obtained by ps pulses. In view of the rapid hydrolysis and oxidation reaction of the newly synthesized NPs with surrounding environment during a very short period of time after ablation, the structure and composition of NPs are changing rapidly and becoming unstable. Therefore, the NPs with stable morphology and structure are selected for the measurement of XRD. The results are shown in figure 5.

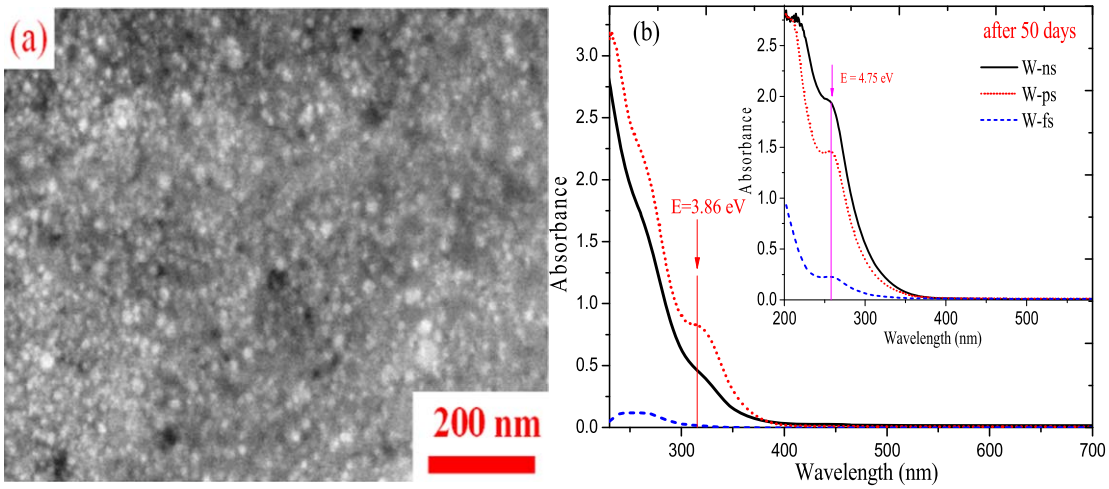

Figure 4. (a) SEM image of W NPs obtained using ps pulses (pulse duration: 200 ps, wavelength: 800 nm, pulse energy: 0.54 mJ, duration of ablation: 40 min). (b) Absorption spectra of aqueous solutions of W NPs obtained using different pulse durations (5 ns, 200 ps and 60 fs). SPR peak position was at $\lambda = 320$ nm (E = 3.86 eV). Inset: absorption spectra after 50 days, and the peak of SPR had a shift to $\lambda = 260$ nm (E = 4.75 eV).

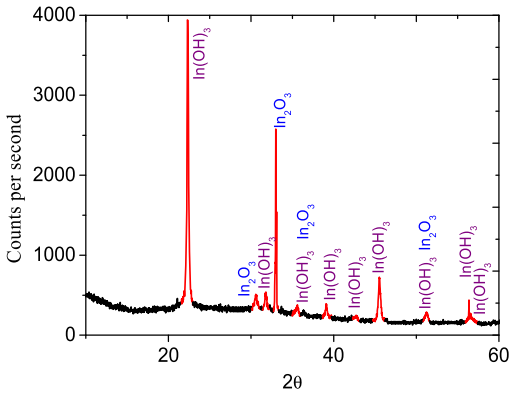

Figure 5. XRD of NPs obtained during In ablation by ps pulses after several days of aging.

Indium can hydrolyze and oxidize with water and oxygen to form $In(OH)_3$ and In_2O_3. The XRD results have confirmed this assumption. In addition, we assumed that most metals in this study can oxidize with oxygen to form metal oxides. Therefore, the colloidal solution obtained by ablation of Sn and Zn is more likely to be a mixture of metal NPs and metal oxide NPs. However, there is no possibility of oxidation and hydrolysis of tungsten because of its high stability.

4. Nonlinear optical studies of NPs suspensions

Ti:sapphire laser (Spitfire Ace, Spectra-Physics, 60 fs pulse duration, 800 nm wavelength, 1 kHz pulse repetition rate) was used as the source for Z-scan studies. The second harmonic of Ti:sapphire laser (400 nm wavelength) was also used in these studies. In the case of OA Z-scans the following formula was used for fitting the experimental data [35]:

$$T(z) = \sum_{m=0}^{\infty} \frac{(-q)^m}{(m+1)^{3/2}} \approx 1 - \frac{q}{2\sqrt{2}} \tag{1}$$

$$q = \frac{\beta I_0 L_{eff}}{1 + z^2/{z_0}^2}$$

Here $T(z)$ is the normalized transmittance along Z-scans, β is the nonlinear absorption coefficient determined in SI units, $L_{\text{eff}} = [1-\exp(-\alpha_0 L)]/\alpha_0$ is the effective length of the medium, α_0 is the linear absorption coefficient, L is the thickness of our samples, z_0 is the Rayleigh length, $z_0 = k(w_0)^2/2$, $k = 2\pi/\lambda$ is the

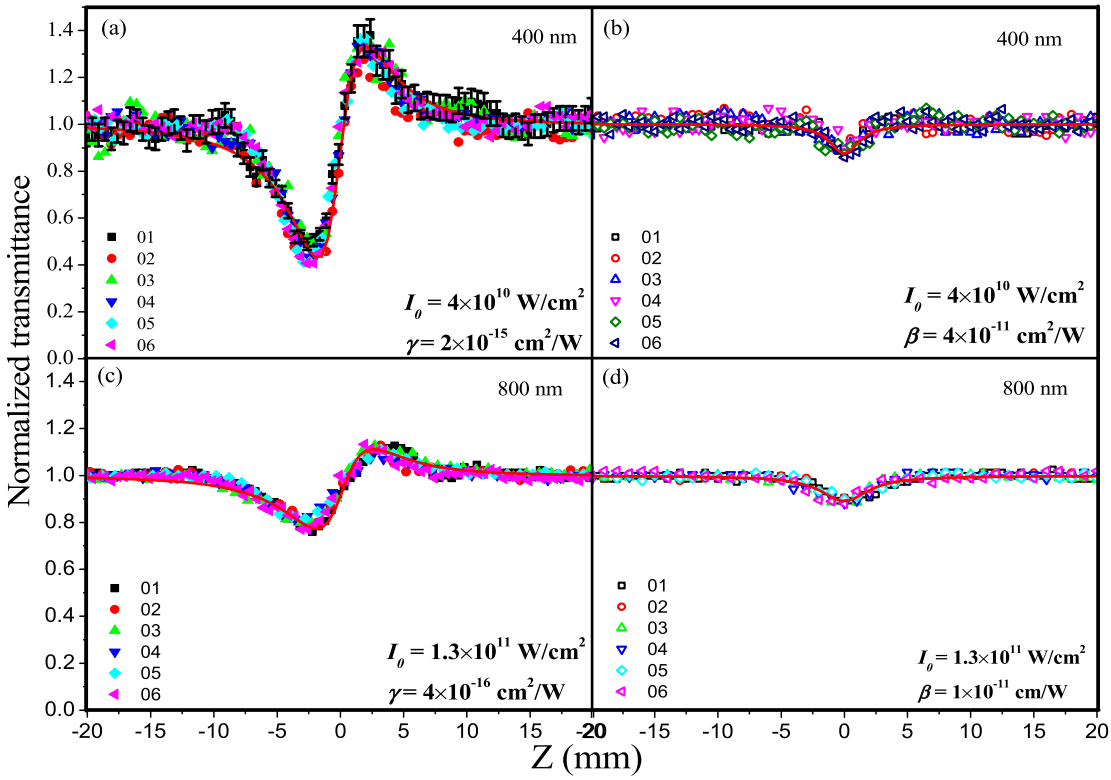

Figure 6. Experimental results (points of different shapes) and theoretical fittings (solid curves) of the Z-scans of NPs solutions obtained by ablated In bulk with different energies of ablation using 60 fs, 1 kHz (a), (b) 400 nm and (c), (d) 800 nm laser pulses (see table 2).

wave number, w_0 is the beam waist radius at the $1/e^2$ level of intensity distribution, and I_0 is the laser radiation intensity in the focal plane. From the fitting the value of $q = \beta I_0 L_{\text{eff}}$ at focal plane (z = 0), one can find the nonlinear absorption coefficient $\beta = q/I_0 L_{\text{eff}}$.

In the case of CA Z-scans the process of nonlinear refraction and absorption is described by [53]

$$T(z) = 1 + \frac{2(-\rho x^2 + 2x - 3\rho)}{(x^2 + 9)(x^2 + 1)}\Delta\Phi_0 \tag{2}$$

where $x = z/z_0$, $\rho = \beta/2k\gamma$, $\Delta\Phi_0 = k\gamma I_0 L_{\text{eff}}$, $\Delta\Phi_0$ *is* the phase change due to nonlinear refraction. The corresponding nonlinear refractive index can be obtained using the relation $\gamma = \Delta\Phi_0/kI_0L_{\text{eff}}$, and $\Delta\Phi_0$ defined from the fitting with experimental data. Then β can be calculated from the ρ determined using the fitting procedure.

Before these experiments, the fused silica cell containing distilled water was tested by the Z-scan at different pulse energies. In that case, we did not observe any nonlinear optical absorption and refraction. Meanwhile, the nonlinear optical response of the aqueous suspension containing metal NPs was observed even at low pulse energy. Therefore it was concluded that the nonlinear optical refraction and absorption of studied colloidal suspension were attributed to the metal NPs.

4.1. In NPs suspensions

Samples 01 to 06 were obtained by ablation In target using different incident energy of ps pulses. The nonlinear optical properties of these samples were studied using 400 (figures 6(a), (b)) and 800 nm (figures 6(c), (d)) fs pulses. Both at 400 or 800 nm no significant difference was observed in OA and CA Z-scan curves of these samples obtained using different pulse ablation energies. SEM images also showed that these NPs have no significant difference in morphology, size and concentration. Meanwhile, the absorption spectra of different samples showed regular changes. Absorption of samples obtained using high pulse energy was significantly stronger compared with the samples obtained using low pulse energy. Obviously, the concentration of In atoms in suspension was increased at higher energies of ablation pulse that led to the growth of a whole absorption. However, the concentration of NPs did not change significantly with increasing the ablation pulse energy. These studies show that the nonlinear optical properties of ablated materials largely depend on the concentration of NPs in suspension, rather than the concentration of atoms or molecules. That is why the Z-scans of samples

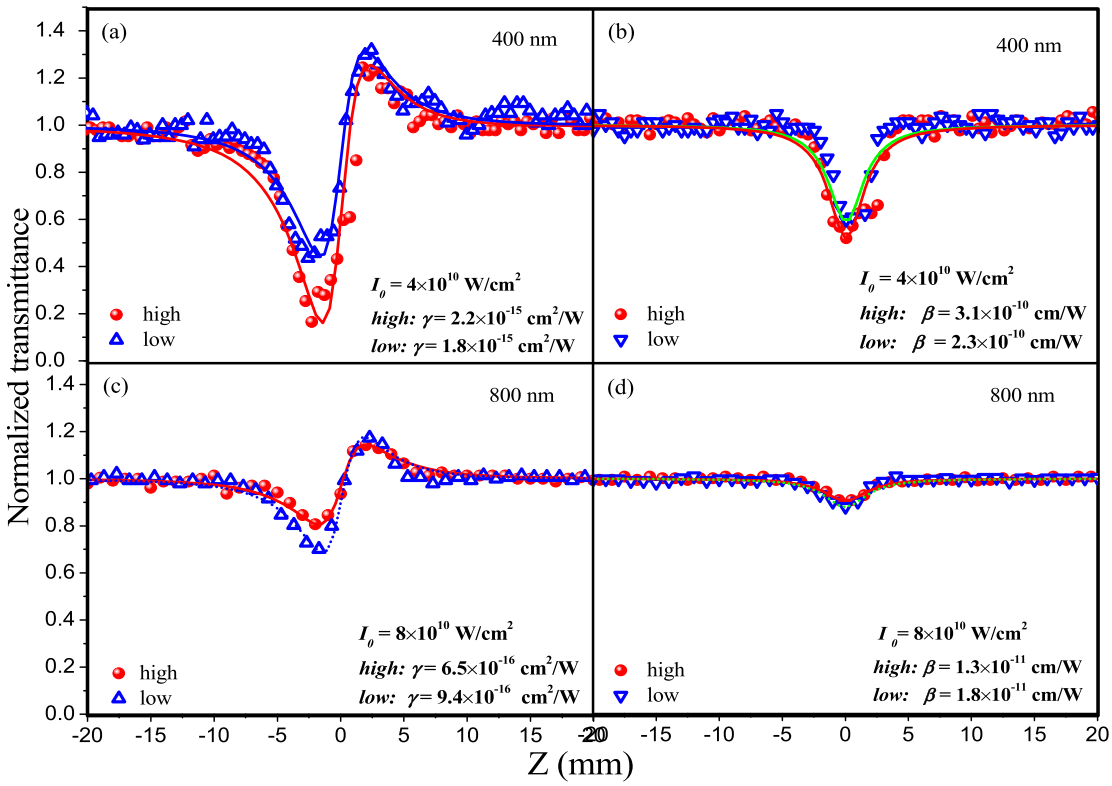

Figure 7. Experimental results and theoretical fittings of CA and OA Z-scans of NPs solutions obtained by ablated In bulk at different temperatures of liquid using 400 (a), (b) and 800 nm (c), (d) 60 fs, 1 kHz laser pulses.

01–06 were similar to each other. The error bars (±5%) of these and other measurements of metal suspensions were the same during entire course of studies. The error bars of the values of γ and β were ±25%.

Under different wavelength conditions, CA Z-scans of all samples showed the self-focusing properties, while OA Z-scans showed the two-photon absorption. In the case of $\lambda = 400$ nm, Z-scans were carried out using the intensity of 4×10^{10} W cm^{-2}. The nonlinear refractive index and nonlinear absorption coefficient were measured to be 2×10^{-15} cm^2 W^{-1} and 4×10^{-11} cm W^{-1} respectively. Meanwhile, at 800 nm, ($I_0 = 1.3 \times 10^{11}$ W cm^{-2}), the corresponding nonlinear characteristics were defined to be a few times smaller ($\gamma = 4 \times 10^{-16}$ cm^2 W^{-1} and $\beta = 1 \times 10^{-11}$ cm W^{-1}).

800 nm fs laser was used at different incident energies to analyze the nonlinear optical properties of sample In-ps06. The results showed that, as for other NPs, its nonlinear optical properties have a strong correlation with incident energy. When we increased the incident intensity from 5×10^{10} W cm^{-2} to 8×10^{10} W cm^{-2} and 11×10^{10} W cm^{-2}, the corresponding nonlinear refractive index was increased from 7.3×10^{-16} to 8.6×10^{-16} and 9.4×10^{-16} cm^2 W^{-1}. The corresponding nonlinear absorption coefficients were measured to be 1.1×10^{-11}, 2.3×10^{-11} and 7×10^{-11} cm W^{-1}. Thus, both γ and β were changed with the growth of incident energy. Notice that there was no linear relationship between these parameters. These observations show that some additional nonlinear optical processes cause the growth of γ and β, since the latter parameters should not depend on incident energy (and, correspondingly, intensity) of the probe pulses if we consider the involvement of solely third-order nonlinearities in the processes of nonlinear refraction and nonlinear absorption.

The ablation of In target in liquid environment was studied at different temperatures of water [high (80 °C) and low (4 °C)]. The nonlinear optical properties of the samples obtained using the same pulse energy and ablation time but at different temperatures of liquid were studied using fs pulses at 400 and 800 nm respectively (figure 7). The results of Z-scans showed that the temperature of water slightly affects the formation of NPs during ablation, thus insignificantly changing the nonlinear optical characteristics of suspension. Particularly, at $\lambda = 400$ nm, $I_0 = 4 \times 10^{10}$ W cm^{-2}, the nonlinear refractive index and nonlinear absorption coefficient of sample obtained at high temperature ($\gamma = 2.2 \times 10^{-15}$ cm^2 W^{-1}, $\beta = 3.1 \times 10^{-10}$ cm W^{-1}) were slightly larger than those obtained at low temperature ($\gamma = 1.8 \times 10^{-15}$ cm^2 W^{-1}, $\beta = 2.3 \times 10^{-10}$ cm W^{-1}). The reverse results were obtained in the case of 800 nm probe fs pulses ($I_0 = 8 \times 10^{10}$ W cm^{-2}). Z-scans showed that γ of the sample obtained at low temperature ($\gamma = 9.4 \times 10^{-16}$ cm^2 W^{-1}) was larger than that of sample obtained at high temperature ($\gamma = 6.5 \times 10^{-16}$ cm^2 W^{-1}). The same was true for OA Z-scan. β of the sample

Table 4. Nonlinear optical parameters of In suspensions.

Wavelength (nm)	I (W cm^{-2})	Sample	β (cm W^{-1})	γ (cm^2 W^{-1})
400	4×10^{10}	In-ps-high	3.1×10^{-10}	2.2×10^{-15}
		In-ps-low	2.3×10^{-10}	1.8×10^{-15}
	4×10^{10}	In-ps01~06	4×10^{-11}	2×10^{-15}
800	1.3×10^{11}		1×10^{-11}	4×10^{-16}
	5×10^{10}	In-ps06	1.1×10^{-11}	7.3×10^{-16}
	8×10^{10}		2.3×10^{-11}	8.6×10^{-16}
	11×10^{10}		7×10^{-11}	9.4×10^{-16}
	8×10^{10}	In-ps-high	1.3×10^{-11}	6.5×10^{-16}
		In-ps-low	1.8×10^{-11}	9.4×10^{-16}
400	4×10^{10}	In-ns	5.4×10^{-11}	2×10^{-15}
800	1.3×10^{11}		1×10^{-11}	6.3×10^{-16}

obtained at low temperature was (1.8×10^{-11} cm W^{-1}) that is higher than β for high temperature (1.3×10^{-11} cm W^{-1}).

Analysis of In NPs suspensions prepared using ns pulses showed that, in the case of 400 nm fs pulses and incident intensity of $I_0 = 4 \times 10^{10}$ W cm^{-2}, the nonlinear refractive index and nonlinear absorption coefficient of samples were 2×10^{-15} cm^2 W^{-1} and 5.4×10^{-11} cm W^{-1} respectively. For the samples prepared using ps pulses the Z-scans (60 fs, 400 nm) showed exactly the same γ, while β was only slightly different (4×10^{-11} cm W^{-1}). In the case of 800 nm pulses ($I = 1.3 \times 10^{11}$ W cm^{-2}) the nonlinear optical properties of the sample prepared using ns pulses were $\gamma = 6.3 \times 10^{-16}$ cm^2 W^{-1} and $\beta = 1 \times 10^{-11}$ cm W^{-1}. The results are basically consistent with the experimental results of the samples prepared using ps pulses.

In the case of ablation by ps pulses with different energy there was no significant difference in morphology, size of particles and concentration of these samples. Their nonlinear refractive indices and nonlinear absorption coefficients were almost the same. Incident pulse intensity, pulse wavelength, as well as temperature of water during ablation slightly influenced the nonlinear optical properties of NPs. The nonlinear optical characteristics of NPs suspensions are collected in table 4.

4.2. Sn, Zn, and W nanoparticle suspensions

The Sn target was ablated to obtain NPs by different pulse durations (5ns, 200ps and 60fs pulses, the corresponding samples are marked as Sn-ns, Sn-ps and Sn-fs respectively). The nonlinear optical properties of Sn suspensions were studied using fs pulses (400 nm, figures 8(a)–(d) and 800 nm, figures 8(e), (f)). In the case of 400 nm radiation the CA Z-scans showed that the nonlinear optical characteristics of different samples have no significant difference at the same intensity of probe pulses (figures 8(a), (b)). The CA Z-scans showed that when the incident intensity increased from $I_0 = 1.5 \times 10^{10}$ W cm^{-2} to $I_0 = 3.3 \times 10^{10}$ W cm^{-2} and $I_0 = 4.4 \times 10^{10}$ W cm^{-2}, the corresponding nonlinear refractive indices became 3×10^{-15}, 2×10^{-15} and 1.7×10^{-15} cm^2 W^{-1} respectively. Thus, the nonlinear refraction slightly decreases with increase of probe pulse intensity. All of the samples showed self-focusing properties. In the case of OA Z-scan the two-photon absorption of 400 nm radiation was observed. We analyzed the samples ablated by long (Sn-ns) and short pulses (Sn-fs). These Z-scans showed no significant difference when using small intensity (figure 8(c)). The increase of probe pulse intensity slightly changed β (figure 8(d)).

In the case of 800 nm pulses the Z-scans notably varied for different ablation conditions compared with the above-described experiments. At the incident intensity $I_0 = 1 \times 10^{11}$ W cm^{-2}, the nonlinear refractive indices of samples prepared by ns, ps and fs pulses were measured to be 1.2×10^{-16}, 1.1×10^{-15} and 1.1×10^{-15} cm^2 W^{-1}, respectively. The corresponding nonlinear absorption coefficients were 1.3×10^{-11}, 4.2×10^{-11} and 6.7×10^{-11} cm W^{-1}. The nonlinear optical properties of the sample prepared by ns pulses became obviously smaller than of those produced by ps and fs pulses. These experimental results showed that at $\lambda = 800$ nm the nonlinear characteristics of these samples have a strong dependence on the duration of the ablation pulse. The nonlinear optical parameters of Sn NPs suspensions are collected in table 5.

The nonlinear refractive indices of Zn-fs and Zn-ns in the case of 400 nm fs pulses had no difference at the same incident intensity (figures 9(a), (b)). The nonlinear refractive index slightly decreased with the growth of probe pulse intensity (from 2.3×10^{-15} cm^2 W^{-1} for $I_0 = 1.5 \times 10^{10}$ W cm^{-2} to 1.5×10^{-15} cm^2 W^{-1} for $I_0 = 3 \times 10^{10}$ W cm^{-2}). In the case of OA Z-scans using 400 nm fs pulses the nonlinear absorption coefficients of different samples were similar to each other and showed some growth with the increase of I_0 (figures 9(c), (d)).

In the case of 800 nm the CA Z-scans also showed insignificant difference in γ of these three samples obtained using different pulse durations. The nonlinear refractive index was 1.5×10^{-15} cm^2 W^{-1}. However, the corresponding nonlinear absorption coefficients at the same incident intensity were 6×10^{-11} cm W^{-1}

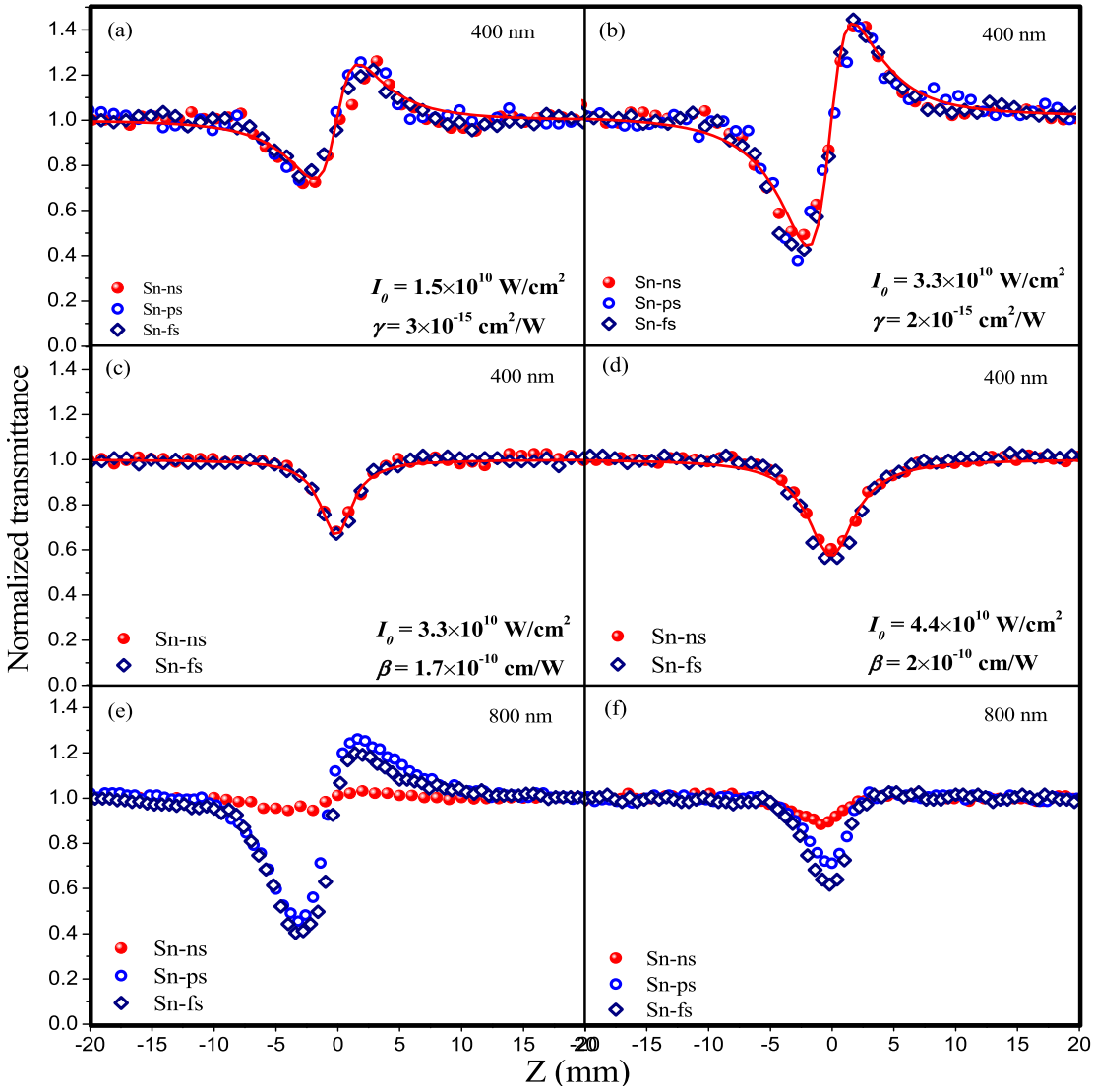

Figure 8. Experimental results and theoretical fittings of CA (a), (b), (e) and OA (c), (d), (f) Z-scans of the Sn NPs solutions obtained by pulses of different duration at 400 (a)–(d) and 800 nm (e), (f), with 60 fs, 1 kHz laser pulses.

Table 5. Nonlinear optical parameters of suspensions of Sn, Zn and W NPs.

	Wavelength (nm)	I (W cm^{-2})	Sample	β (cm W^{-1})	γ (cm^2 W^{-1})
Sn	400	3.3×10^{10}	Sn-ns/ps/fs	1.7×10^{-10}	2.3×10^{-15}
	800	1×10^{11}	Sn-ns	1.3×10^{-11}	1.2×10^{-16}
			Sn-ps	4.2×10^{-11}	1.1×10^{-15}
			Sn-fs	6.7×10^{-11}	1.1×10^{-15}
Zn	400	3×10^{10}	Zn-ns/ps/fs	1.5×10^{-10}	2×10^{-15}
	800	8×10^{10}	Zn-ns	6×10^{-11}	1.5×10^{-15}
			Zn-ps	3.4×10^{-11}	
			Zn-fs	2.8×10^{-11}	
W	800	8×10^{10}	W-ns	1.2×10^{-10}	1.7×10^{-15}
			W-ps	3×10^{-11}	1.3×10^{-15}
			W-fs		1.2×10^{-15}

(Zn-ns), 3.4×10^{-11} cm W^{-1} (Zn-ps) and 2.8×10^{-11} cm W^{-1} (Zn-fs) respectively. The relation between the incident intensity and the nonlinear absorption coefficient was studied using OA Z-scans of the samples prepared by fs pulses. It was shown that the increase of the incident intensity led to the increase of the nonlinear absorption coefficient [at $I = 6.7 \times 10^{10}$ W cm^{-2}, $\beta = 2.1 \times 10^{-11}$ cm W^{-1} and at $I = 1 \times 10^{11}$ W cm^{-2},

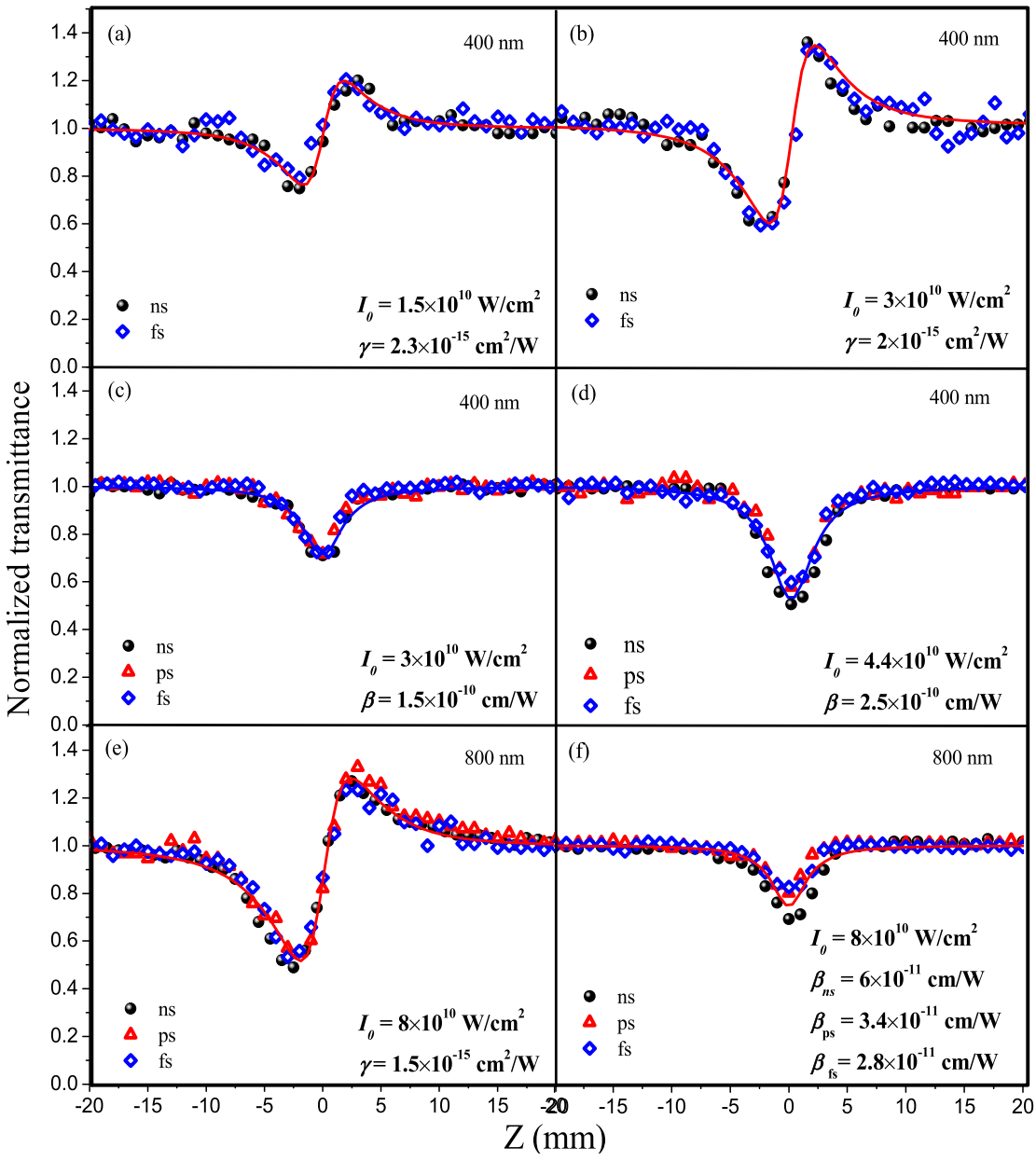

Figure 9. Experimental results and theoretical fittings of CA (a), (b), (e) and OA (c), (d), (f) Z-scans of Zn NPs solutions obtained by pulses of different duration at 400 (a)–(d) and 800 nm (e), (f), with 60 fs, 1 kHz laser pulses.

$\beta = 4.7 \times 10^{-11}$ cm W^{-1}]. The nonlinear optical characteristics of suspensions of Zn NPs are collected in table 5.

The nonlinear optical properties of the suspensions of W NPs synthesized using different pulses (ns, ps and fs) were studied using 800 nm fs pulses. The CA Z-scans showed self-focusing, while OA Z-scan showed two-photon absorption (figure 10). The nonlinear refractive indices of three samples (W-ns, W-ps and W-fs) showed very small difference ($\gamma \approx 1.3 \times 10^{-15}$ cm^2 W^{-1}). The OA Z-scans showed that the nonlinear absorption coefficients of samples obtained using ps and fs pulses are exactly the same ($\beta = 3 \times 10^{-11}$ cm W^{-1}), while the sample prepared using ns pulses had significantly larger two-photon absorption ($\beta = 1.2 \times 10^{-10}$ cm W^{-1}).

The prepared using ns pulses sample was used to analyze the relation between the intensity of 800 nm pulses and the nonlinear refractive index. It was shown that the increase of pulse intensity leads to small decrease in nonlinear refractive index. We also studied the relation between pulse intensity and nonlinear absorption, and showed some growth of β with the increase of incident intensity. In most cases the variations of nonlinear optical parameters at different probe intensities were close to the errors of our measurements. The measurements of γ and β of W nanoparticle suspensions are collected in table 5.

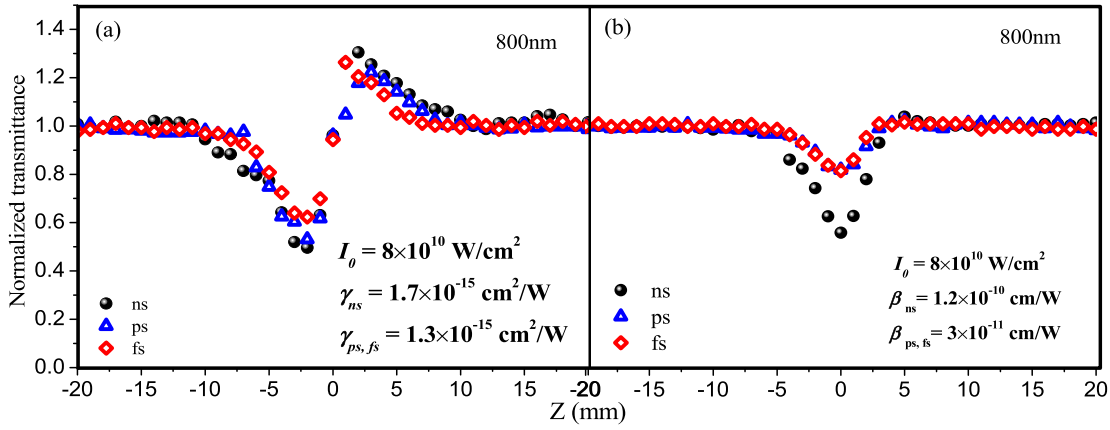

Figure 10. Experimental results and theoretical fittings of CA (a) and OA (b) Z-scans of W NPs solutions obtained by pulses of different duration at 800 nm, with 60 fs, 1 kHz laser pulses.

5. Conclusions

In this paper four metals (In, Sn, Zn and W) with different hardness and melting point were ablated by pulsed laser in liquid environment to synthesize different suspensions of NPs. The influence of pulse duration, pulse energy and temperature of liquid on the formation of NPs was analyzed.

The results show that the pulse energy and temperature of liquid environment have little effect on the formation of NPs for the metal which has smaller hardness (In). Small hardness and melting point make it extremely easy to be ablated, resulting in a wide range of ablation conditions can achieve similar ablation effect. Therefore, their nonlinear optical properties were also similar. However, pulse duration plays a very important role during the formation of NPs, especially in the influence of particle size. It is found that ultra-short pulses have a positive effect in the acquisition of smaller particles. This conclusion is not affected by the hardness of metal.

In addition, for metals (Sn, Zn) with medium hardness, the influence of pulse duration on laser ablation was more significant. Not only the morphology and size of NPs, but also the nonlinear optical properties were changed in this case. Size variation of NPs of ablated metal with high hardness (W) showed that pulse duration had significant influence on the morphology. We have shown that incident intensity and wavelength of the fs laser affects the nonlinear optical properties of the produced NPs.

Acknowledgments

The financial support from Natural Science Foundation of China (NSFC, 21404015, 61774155, 61705227), National Key Research and Development Program of China (2017YFB1104700), and Jilin Science and Technology Department Project (20150204019GX) is appreciated. R A G thanks the financial support from Chinese Academy of Sciences President's International Fellowship Initiative (Grant No. 2018VSA0001).

ORCID iDs

Ke Zhang https://orcid.org/0000-0003-2793-552X
Rashid A Ganeev https://orcid.org/0000-0001-5522-1802
Pavel V Redkin https://orcid.org/0000-0002-7436-5614

References

[1] Blum O and Shaked N T 2015 Prediction of photothermal phase signatures from arbitrary plasmonic NPs and experimental verification *Light: Sci. Appl* **4** e322
[2] Karabchevsky A, Mosayyebi A and Kavokin A V 2016 Tuning the chemiluminescence of a luminol flow using plasmonic NPs *Light: Sci. Appl* **5** e16164
[3] Su Y H, Ke Y F, Cai S L and Yao Q Y 2012 Surface plasmon resonance of layer-by-layer gold NPs induced photoelectric current in environmentally-friendly plasmon-sensitized solar cell *Light: Sci. Appl* **1** e14
[4] Chen X, Jia B, Zhang Y and Gu M 2013 Exceeding the limit of plasmonic light trapping in textured screen-printed solar cells using Al NPs and wrinkle-like graphene sheets *Light: Sci. Appl* **2** e92

[5] Wang K, Zhou J, Yuan L, Tao Y, Chen J, Lu P and Wang Z L 2012 Anisotropic third-order optical nonlinearity of a single ZnO micro/nanowire *Nano Lett.* **12** 833–8
[6] Seo J T *et al* 2009 Optical nonlinearities of Au NPs and Au/Ag coreshells *Opt. let.* **34** 307–9
[7] Feng Y, Yao Q, Li J, Goswami N, Xie J and Yang J 2016 Converting ultrafine silver nanoclusters to monodisperse silver sulfide nanoparticles via a reversible phase transfer protocol *Nano Research* **9** 942–50
[8] Ganeev R A, Ryasnyansky A I, Kamalov S R, Kodirov M K and Usmanov T 2001 Nonlinear susceptibilities, absorption coefficients and refractive indices of colloidal metals *J. Phys. D: Appl. Phys.* **34** 1602–11
[9] Gan J *et al* 2013 Oxygen vacancies promoSng photoelectrochemical performance of In_2O_3 nanocubes *Sci. Rep.* **3** 1021
[10] Salem E T 2012 Sn oxide NPs prepared using liquid phase laser ablation for optoelectronic application *Nanoscience and Nanotechnology* **2** 86–9
[11] Dali S, Liqiao Q and High S S 2012 Responsivity, bandpass near-UV photodetector fabricated from PVA-In_2O_3 NPs on a GaN substrate *IEEE Photo J.* **4** 715–20
[12] Zhang D, Li C, Han S, Liu X, Tang T, Jin W and Zhou C 2003 Ultraviolet photodetection properties of In oxide nanowires *Appl. Phys.* A **76** 1–4
[13] Li F, Jian J, Wu R, Li J and Sun Y 2015 Synthesis, electrochemical and gas sensing properties of In_2O_3 nanostructures with different morphologies *J. Alloys and Compounds.* **645** 178–83
[14] Zhang S, Song P, Yan H and Wang Q 2016 Self-assembled hierarchical Au-loaded In_2O_3 hollow microspheres with superior ethanol sensing properties *Sensors and Actuators B: Chem.* **231** 245–55
[15] Lee D, Ondrake J and Cui T 2011 A conductometric In oxide semiconducSng nanoparticle enzymatic biosensor array *Sensors* **11** 9300–12
[16] Kim K M, Choi K I, Jeong H M, Kim H J, Kim H R and Lee J H 2012 Highly sensitive and selective trimethylamine sensors using Ru-doped SnO_2 hollow spheres *Sensors and Actuators B: Chem.* **166** 733–8
[17] Xie Z, Zhao J and Wang Y 2015 One-step solvothermal synthesis of Sn NPs dispersed in ternary manganese-nickel-cobalt carbonate as superior anode materials for lithium ion batteries *Electrochim. Acta* **174** 1023–9
[18] Manikandan K, Dhanuskodi S, Maheswari N and Muralidharan G 2016 SnO_2 nanoparticles for supercapacitor application *AIP Conf. Proc.* **1731** 050048-1–050048-3
[19] Zhu Z, Wang S, Du J, Jin Q, Zhang T, Cheng F and Chen J 2014 Ultrasmall Sn NPs embedded in nitrogen-doped porous carbon as high-performance anode for lithium-ion batteries *Nano Lett.* **14** 153–7
[20] Janotti A and Van de Walle C G 2009 Fundamentals of Zn oxide as a semiconductor *Rep. Prog. Phys.* **72** 126501
[21] Kozuka Y, Tsukazaki A and Kawasaki M 2014 Challenges and opportunities of ZnO-related single crystalline heterostructures *Appl. Phys. Rev.* **1** 011303
[22] Usui H, Shimizu Y, Sasaki T and Koshizaki N 2005 Photoluminescence of ZnO NPs prepared by laser ablation in different surfactant solutions *J. Phys. Chem.* B **109** 120–4
[23] Lakshmi Prasanna V and Vijayaraghavan R 2017 Chemical manipulation of oxygen vacancy and antibacterial activity in ZnO *Mater. Sci. Eng.* C **77** 1027–34
[24] Zhang Z Y and Xiong H M 2015 Photoluminescent ZnO NPs and their biological applications *Materials.* **8** 3101–27
[25] Gurlo A, Ivanovskaya M, Barsan N, Schweizer-Berberich M, Weimar U and Gopel W 1997 Grain size control in nanocrystalline In_2O_3 semiconductor gas sensors *Sensors and Actuators B: Chem.* **44** 327–33
[26] Rey J F Q, Plivelic T S, Rocha R A, Tadokoro S K, Torriani I and Muccillo E N S 2005 Synthesis of In_2O_3NPs by thermal decomposition of a citrate gel precursor *J. Nano. Res.* **7** 203–8
[27] Patra C R and Gedanken A 2004 Rapid synthesis of NPs of hexagonal type In_2O_3 and spherical type Tl_2O_3 by microwave irradiation *New J. Chem.* **28** 1060–5
[28] Ryzhikov A S, Vasiliev R B, Rumyantseva M N, Ryabova L I, Dosovitsky G A, Gilmutdinov A M, Kozlovsky V F and Gaskov A M 2002 Microstructure and electrophysical properties of SnO_2, ZnO and In_2O_3 nanocrystalline films prepared by reactive magnetron sputtering *Mater. Sci. and Eng.* B **96** 268–74
[29] Yamamoto T, Machib K, Nagareb S, Hamadab K and Senna M 2004 The relation between surface plasmon resonance and morphology of Ag nanodots prepared by pulsed laser deposition *Solid State Ion.* **172** 299–302
[30] Beena D, Vinodkumar R, Navas I, Rajan G and Mahadevan Pillai V P 2010 Efficient photoluminescence from pulsed laser ablated nanostructured In oxide films *Mater. Sci. and Eng.* B **174** 59–65
[31] Dorranian D, Tajmir S and Khazanehfar F 2013 Effect of Laser Fluence on the Characteristics of Ag NPs Produced by Laser Ablation *Soft Nanoscience Lett.* **03** 93–100
[32] Chen Y H and Yeh C S 2002 Laser ablation method: use of surfactants to form the dispersed Ag NPs *Coll and Surf* A **197** 133–9
[33] Acacia N, Barreca F, Barletta E, Spadaro D, CurròG and Neri F 2010 Laser ablation synthesis of In oxide NPs in water *Appl. Sur. Sci.* **256** 6918–22
[34] Tsuji T, Thang D H, Okazaki Y, Nakanishi M, Tsuboi Y and Tsuji M 2008 Preparation of silver NPs by laser ablation in polyvinylpyrrolidone solutions *Appl. Sur. Sci.* **254** 5224–30
[35] Sheik-Bahae M, Said A A, Wei T, Hagan D J and Stryland E W V 1990 Sensitive measurement of optical nonlinearities using a single beam *IEEE J. quant elect.* **26** 760–9
[36] Ganeev R A, Rao K S, Yu Z, Yu W, Yao C, Fu Y, Zhang K and Guo C 2018 Strong nonlinear absorption in perovskite films *Opt. Mate. Exp.* **8** 1472
[37] George A, Choudhary H K, Satpati B and Mandal S 2015 Synthesis, characterization and optical properties of ligand-protected In nanoparticles *Phys. Chem.* **17** 7109–13
[38] Zhao Y, Zhang Z and Dang H 2003 A Novel Solution Route for Preparing In NPs *J. Phys. Chem.* B **107** 7574–6
[39] Khanna P K, Jun K W, Hong K B, Baeg J O, Chikate R C and Das B K 2005 Colloidal synthesis of In NPs by sodium reduction method *Mater. Lett.* **59** 1032–6
[40] Shubina T V, Plotnikov D S, Vasson A, Leymarie J, Larsson M and Holtz P O 2006 Surface-plasmon resonances in In nitride with metal-enriched nano-particles *J. Crystal Growth.* **288** 230–5
[41] Bohren C F and Huffman D R 1983 *Absorption and Scattering of Light by Small Particles* (New York: Wiley)
[42] Zeng H, Cai W, Li Y, Hu J and Liu P 2005 Composition/structural evolution and optical properties of ZnO/Zn NPs by laser ablation in liquid media *J. Phys. Chem.* B **109** 18260–6
[43] Srikant V and Clarke D R 1998 On the optical band gap of Zn oxide *J. Appl. Phys.* **83** 5447–51
[44] Kim K K, Kim D, Kim S K, Park S M and Song J K 2011 Formation of ZnO NPs by laser ablation in neat water *Chem. Phys. Lett.* **511** 116–20

[45] Gondal M A, Drmosh Q A, Yamani Z H and Saleh T A 2009 Synthesis of ZnO_2 NPs by laser ablation in liquid and their annealing transformation into ZnO NPs *Appl. Surf. Sci.* **256** 298–304
[46] Camarda P, Vaccaro L, Messina F and Cannas M 2015 Oxidation of Zn NPs probed by online optical spectroscopy during ns pulsed laser ablation of a Zn plate in H_2O *Appl. Phys. Lett.* **107** 013103
[47] Acsente T, Negrea R F, Nistor L C, Logofatu C, Matei E, Birjega R, Grisolia C and Dinescu G 2015 Synthesis of flower-like W NPs by magnetron sputtering combined with gas aggregation *The European Phys J D.* **69** 161
[48] Acsente T, Negrea R F, Nistor L C, Matei E, Grisolia C, Birjega R and Dinescu G 2017 W NPs with controlled shape and crystallinity obtained by magnetron sputtering and gas aggregation *Mater. Lett.* **200** 121–4
[49] Kamal S S K, Sahoo P K, Vimala J, Shanker B, Ghosal P and Durai L 2016 Synthesis of high purity W NPs from W heavy alloy scrap by selective precipitation and reduction route *J. Alloys Compounds.* **678** 403–9
[50] Khani A H, Rashidi A M and Kashi G 2017 Synthesis of W NPs by reverse micelle method *J. Molecular Liquids* **241** 897–903
[51] Sahoo P K, Kalyan Kamal S, Premkumar M, Jagadeesh Kumar T, Sreedhar B, Singh A K, Srivastava S K and Sekhar K C 2009 Synthesis of W NPs by solvothermal decomposition of W hexacarbonyl *Int. J. Refractory Metals and Hard Materials.* **27** 784–91
[52] Sarmah T, Aomoa N, Bhattacharjee G, Sarma S, Bora B, Srivastava D N, Bhuyan H, Kakati M and Temmerman G D 2017 Plasma expansion synthesis of W nanopowder *J. Alloys and Compounds.* **725** 606–15
[53] Liu X, Guo S, Wang H and Hou L 2001 Theoretical study on the closed-aperture Z-scan curves in the materials with nonlinear refaction and strong nonlinear absorption *Opt. Commun.* **197** 431–7